Superlattices and Microstructures, Vol. 26, No. 3, 1999
Article No. spmi.1999.0772
Available online at http://www.idealibrary.com on IDEAL

Modification of the lattice thermal conductivity in silicon quantum wires due to spatial confinement of acoustic phonons

A. KHITUN†, A. BALANDIN‡, K. L. WANG
Device Research Laboratory, Electrical Engineering Department, University of California-Los Angeles, Los Angeles, CA 90095-1594, U.S.A.

(Received 15 July 1999)

Lattice thermal conductivity in silicon quantum wires is theoretically investigated. The bulk of heat in silicon structures is carried by acoustic phonons within a small region in the first Brillouin zone. Our formalism rigorously takes into account modification of these acoustic phonon modes and phonon group velocities in free- and clamped-surface wires due to spatial confinement. From our numerical results, we predict a significant decrease (more than an order of magnitude) of the lattice thermal conductivity in cylindrical quantum wires with diameter $D = 200$ Å. The decrease is about two times stronger in quantum wires than in quantum wells of corresponding dimensions. Our theoretical results are in qualitative agreement with experimentally observed drop of the lattice thermal conductivity in silicon low-dimensional structures.

Key words: thermal conductivity, confined phonons, quantum wires.

1. Introduction

The development of sophisticated pattering and self-assembly techniques for quasi one-dimensional (1D) semiconductor structures (quantum wires) [1, 2] has stimulated a large body of new work in semiconductor physics over the last 10 years. Quantum wires with widths down to 100 Å and small size fluctuations have been fabricated by regular electron beam lithography and wet etching [3]. Much of this interest into quantum wires was further stimulated by the possibility of novel 'low-dimensional' physics related to spatial confinement of carriers and phonons [4, 5], as well as applications in electronic and optoelectronic devices.

Recently, it has been suggested that the thermoelectric figure of merit $ZT = S^2\sigma/(k_{ph} + k_e)$ can be significantly enhanced in quantum wells [6] and quantum wires [7] because of strong carrier confinement (where S is the Seeback coefficient, σ is the electric conductivity, k_{ph} is the lattice thermal conductivity, and k_e is the electronic thermal conductivity). An increase to the thermoelectric figure of merit may also come from the drop of the lattice thermal conductivity in low-dimensional structures due to the increased phonon–boundary scattering [8]. Experimental evidence of the thermal conductivity drop in thin Si films has also been demonstrated [9]. Some of us have also shown that an additional increase to ZT can be brought by the spatial confinement of acoustic phonons in thin quantum well structures embedded within material of distinctively

†E-mail: ahit@ee.ucla.edu

‡Present address: Department of Electrical Engineering, University of California, Riverside, CA 92521, U.S.A.

0749–6036/99/090181 + 13 $30.00/0

different elastic properties [10]. Thus, low-dimensional confinement of both carriers and phonons allows for more degrees of freedom for maximizing ZT.

The experimentally observed increase of the Seebeck coefficient in SiGe/Si multiple-quantum well structures has already given confirmation of the advantages of low dimensionality [11]. To date, most of the experimental attempts to attain increased thermoelectric characteristics in low-dimensional structures were carried out with semiconductor superlattices or multiple-quantum well structures. Utilization of quantum wires for thermoelectric applications would require a two-dimensional array of quantum wires fabricated using e-beam lithography or self-assembly techniques. Difficulties of high-quality fabrication of such an array explain the scarcity of the experimental data for quantum wires.

As a prototype system for theoretical study of thermal conductivity we have chosen silicon quantum wires. This choice was made for two reasons. Firstly, Si/Ge material systems (in its bulk or nanostructured form) have already shown a great promise for high-temperature thermoelectric applications. Secondly, the problem of lattices thermal conductivity in silicon quantum wires is also important in a view of continuous down scaling of the device feature size, which may lead to the increased heat dissipation per unit area. Further development of the deep-submicron technology makes the problem of heat management of nano-size silicon structures particularly acute.

In this paper we investigate the lattices thermal conductivity in a generic cylindrical silicon quantum wire taking into account modification of the acoustic phonon modes and phonon group velocities in free- and clamped-surface wires due to spatial confinement effects. At room temperature and above, acoustic phonons, with the wavevectors close to the Brillouin zone center, carry most of the heat in silicon bulk material and low-dimensional structures. Our model rigorously takes into account all phonon scattering processes important for silicon wires including mass-difference, Umklapp, and Casimir-limit boundary scattering. The rest of the paper is organized as follows. In Section 2, we present our theoretical model for the thermal conductivity. Calculation of acoustic phonon group velocities for free- and clamped-surface quantum wires is given in Section 3. The results of numerical simulation of the thermal conductivity and discussion are in presented in Section 4 and Section 5, respectively and the conclusions will be given in Section 6.

2. Theory

Thermal conductivity of semiconductors is the sum of the lattice (phonon) k_{ph} and electronic k_e components. The maximum value of the thermoelectric figure of merit is usually obtained for doped semiconductors when $k_e/k_{ph} \sim \frac{1}{2}$ [12], although this ratio for an intrinsic silicon wire is even lower. For simplicity, in this paper we limit our consideration to the lattice (phonon) contribution to the thermal conductivity and neglect its electronic part.

It is well known that the lattice thermal conductivity is written as [13] $k_{ph} = (\frac{1}{3})\Sigma S(\omega) v_g \Lambda(\omega) d\omega$, where $S(\omega)$ is the contribution to the specific heat per frequency interval from phonons of frequency w, $\Lambda(\omega)$ is the phonon mean-free-path (attenuation length), and v_g is the phonon group velocity. Using the relaxation-time methods by following Klemen's [13] and Callaway's [14] derivation, the expression for k_{ph} can be further rewritten as

$$k_{ph} = \frac{k_B}{2\pi^2 v_g}\left(\frac{k_B}{\hbar}\right)^3 T^3 \int_0^{\frac{\theta}{T}} \frac{\tau_C x^4 e^x}{(e^x-1)^2} dx, \tag{1}$$

where $x = \hbar\omega/k_B T$, k_B is the Boltzmann constant, $\hbar$ is the Plank constant, θ is the Debye temperature, τ_C is the combined relaxation time, and v_g is the phonon group velocity. Equation (1) is valid under the assumption that the resistive scattering mechanisms, which do not conserve crystal momentum, are dominant. These are the processes that contribute to the lattice thermal resistance. The general expression for the lattice thermal conductivity, which includes an additional term for the normal scattering processes, can be found in Refs [13, 14].

The combined scattering relaxation time is found from Matthiessen's rule

$$\frac{1}{\tau_C} = \frac{1}{\tau_U} + \frac{1}{\tau_B} + \frac{1}{\tau_M} + \frac{1}{\tau_R}, \tag{2}$$

where τ_C is the combined relaxation time due to different scattering mechanisms which are dominant in silicon at room temperature and above. Particularly, the mechanisms include Umklapp scattering (τ_U), boundary scattering (τ_B), mass-difference (or isotope) scattering (τ_M) and resonant scattering for silicon with a high concentration of impurity atoms. In order to determine the lattice thermal conductivity, we calculate all phonon relaxation times in a low-dimensional structure taking into account their modification due to spatial confinement of phonon modes. In the following, we outline all these mechanisms.

Mass-difference scattering arises due to the presence of atoms with a mass different from the average atomic mass in a semiconductor. Different mass can come from isotopes of a particular element or impurity atoms. In the latter case, the difference in stiffness constants between the impurity–host atoms and the host–host atoms, as well as the difference in the atomic volume of the impurity atoms should also be included in the phonon scattering rate expression. We use the standard formula for the mass-difference scattering but introduce one important modification—group velocity dependence on the structure geometry and boundary conditions. The mass-difference scattering rate can be written as [12, 13],

$$\frac{1}{\tau_M} = \frac{V_0 \omega^4}{4\pi v_g^3} \Gamma_M,$$

where the form-factor Γ_M is given as

$$\Gamma_M = f_i[(\Delta M_i/\overline{M})^2 + 2\{(\Delta G_i/G) - 6.4\gamma(\Delta\delta_i/\overline{\delta})\}^2]. \tag{3}$$

Here V_0 is the volume per atom, ω is the phonon frequency, f_i is the fractional content of atoms with mass M_i, which is different from the mass M of the main atom, G_i is the average stiffness constant of the nearest-neighbor bonds from the impurity to the host atom and G corresponding quantity for the host, δ_i is the cube root of the atomic volume for the ith impurity in its own lattice, γ represents the average anharmonicity of the bonds, $\Delta M_i = M - M_i$, and $\overline{M}$ and δ are given as

$$\overline{M} = \sum_i f_i M_i, \qquad \overline{\delta} = \sum_i f_i \delta_i'.$$

The above equations were derived for a regular bulk semiconductor. We extended them to a low-dimensional structure assuming that a quantum wire has finite radius. Phonon confinement effects enter eqn (3) through modification of the phonon group velocity, which has to be calculated for each particular geometry and boundary conditions. In the limiting case of strictly one-dimensional (1D) structure the phonon frequency dependence in eqn (3) changes to $1/\tau_M \sim \omega^2$ [13]. We will not consider this case and limit our analysis to the realistic situation with wire diameter $D \sim 200$ Å or larger. Since in nature silicon always contains a mixture of three main isotopes (92% of ^{28}Si, 4.6% of ^{29}Si, 3.1% of ^{30}Si), the isotope scattering significantly contributes to the thermal resistance of the material.

The boundary scattering in our model is treated in the Casimir limit in that all phonons that have a positive normal velocity lose the sense of their directionality and obey the equilibrium distribution when they reach the boundary [15]. It can be shown that the effective boundary mean free path for a cylindrical quantum wire of diameter D in the Casimir limit is given by $L_0 = D$ [15]. (For a rectangular quantum wire with a square cross-section with side W, the Casimir limit mean free path is $L_0 = 1.12W$). Thus, we write the phonon–boundary scattering rate for a cylindrical quantum wire as

$$\frac{1}{\tau_B} = \frac{v_g}{D}. \tag{4}$$

Resonance scattering is a process in which phonons interact with some localized modes. Under certain conditions, the impurities or point defects in a host semiconductor, which have some internal frequency of oscillation ω_0, can give rise to the resonance absorption on this resonance frequency [16]

$$\frac{1}{\tau_R} = \frac{R\omega^2}{(\omega_0^2 - \omega^2)^2 + \Omega\omega_0^2\omega^2}, \tag{5}$$

where R depends upon the concentration of the impurities (point defects) and Ω is related to damping. We will illustrate the resonant scattering effects using a silicon–germanium materials system as an example.

The expression for the three-phonon Umklapp scattering rate $1/\tau_U$ was obtained by Klemens in the single-mode relaxation time approximation [13]. The modification of the three-phonon Umklapp scattering processes due to the spatial confinement of phonon was treated in details by Balandin and Wang for free-surface thin silicon films (quantum wells) [17]. The situation is analogous in our wire case here with the only exception for different phonon dispersion in quantum wires.

In order to evaluate relaxation rates of eqns (3)–(5), one should use the actual dispersion relations and group velocities, $v_g \equiv v_g(\omega(q))$, for phonons in the free-surface and clamped-surface quantum wires. The modification of wavevector selection and frequency conservation rules due to the spatial confinement should also be taken into account while dealing with the Umklapp processes [18].

3. Phonon group velocities in quantum wires

Most of the heat in silicon at room temperature or above is carried by the acoustic phonons with the wavevectors q close to the center of the Brillouin zone. In this region of the q-vector space, we can determine the phonon dispersion in the elastic continuum approximation. In order to calculate the phonon dispersion and phonon group velocities, which is more important for our model, we solve the elasticity equation using the regular approach outlined in Refs [18, 19]. The elasticity equation is written in a vector form as follows

$$\frac{\partial^2 \boldsymbol{u}}{\partial t^2} = s_t^2 \nabla^2 \boldsymbol{u} + (s_l^2 - s_t^2)\ \text{grad div}\ \boldsymbol{u}, \tag{6}$$

where $s_l = (\lambda + 2\mu)/\rho$ and $s_t = \mu/\rho$ are the velocities of longitudinal and transverse acoustic phonon modes in bulk semiconductor and λ, μ, ρ are Lame constants and ρ is the density. We consider a cylindrical wire of infinite length in the z direction and with a diameter D (see Fig. 1). For simplicity it is assumed that the material of a wire has an isotropic symmetry and it does not have the azimuthal dependency. The components of the stress tensor are written as

$$\begin{aligned} \sigma_{zz} &= \lambda\left(\frac{\partial u_r}{\partial r} + \frac{u_r}{r} + \frac{\partial u_z}{\partial z}\right) + 2\mu\frac{\partial u_r}{\partial r}, \\ \sigma_{rz} &= \mu\left(\frac{\partial u_r}{\partial z} + \frac{\partial u_z}{\partial r}\right). \end{aligned} \tag{7}$$

We consider longitudinal and shear modes of the confined acoustic phonons because of their dominant contributions to the lattice heat transport. The longitudinal acoustic waves have the displacements are given by [19]

$$\begin{aligned} u_r(r, z) &= \left[\frac{d}{dr}\{B J_0(q_l r) + A J_0(q_t r)\}\right] e^{i(qz - \omega t)}, \\ u_z(r, z) &= i\left[q B J_0(q_l r) + \frac{-q_t^2}{q} A J_0(q_t r)\right] e^{i(qz - \omega t)}, \end{aligned} \tag{8}$$

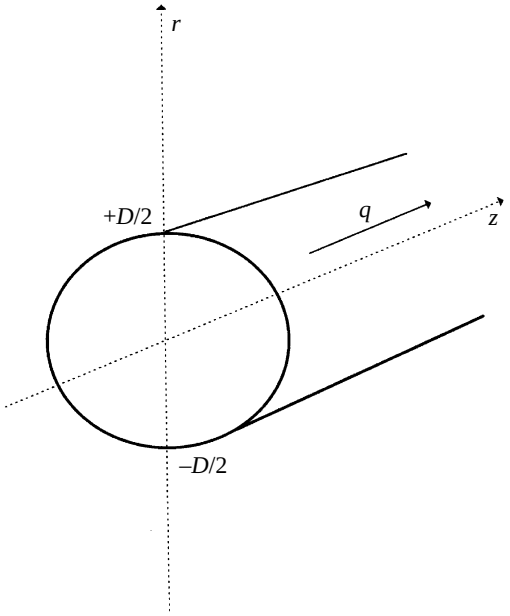

Fig. 1. Geometry of the structure used for model simulations.

where J_0 and J_1 are ordinary Bessel functions, A and B are constants to be determined, and q is the z-component wavevector (direction of propagation). In addition, parameters q_l and q_t are related to the phonon frequency as

$$\omega = s_l\sqrt{q_x^2 + q_l^2} = s_t\sqrt{q_x^2 + q_t^2}. \tag{9}$$

The longitudinal waves are the coupled modes of the axial and radial modes that have the wavevectors q_l and q_t, respectively.

For share waves we have a simple expression

$$u_r(r, z) = J_1(q_t r)e^{i(qz-\omega t)}. \tag{10}$$

This phonon mode has only one nonzero component, which is perpendicular to the direction of wave propagation (z).

We will consider the both cases of boundary conditions: free-surface boundary, and clamped-surface boundary. The free-surface boundary exactly corresponds to the boundary between an elastic material and vacuum, but can be used for a 'rigid' material embedded within 'softer' material. In this case the normal components of the stress tensor are vanish and the displacement is unrestricted:

$$\sigma_{z,z} = \sigma_{r,z} = 0, \qquad \text{at } r = \pm D/2. \tag{11}$$

The rigidity of the material can be quantitatively characterized by its characteristic phonon frequency $\Omega = (4F/M)^{1/2}$. Since $\Omega(\text{Si}) = 40.9$ meV and $\Omega(\text{Ge}) = 22.9$ meV, we can consider silicon wire embedded within germanium to have near-free surface boundary conditions. The ideal example of the free-surface silicon wire is the silicon whiskers grown by vapor–liquid–solid phase MBE [4]. The clamped-surface boundary conditions describe the case of the quantum wire made out of the 'softer' material embedded within perfectly rigid material. In this case boundary conditions take the form

$$u_r = u_z = 0, \qquad \text{at } r = \pm D/2. \tag{12}$$

[t]

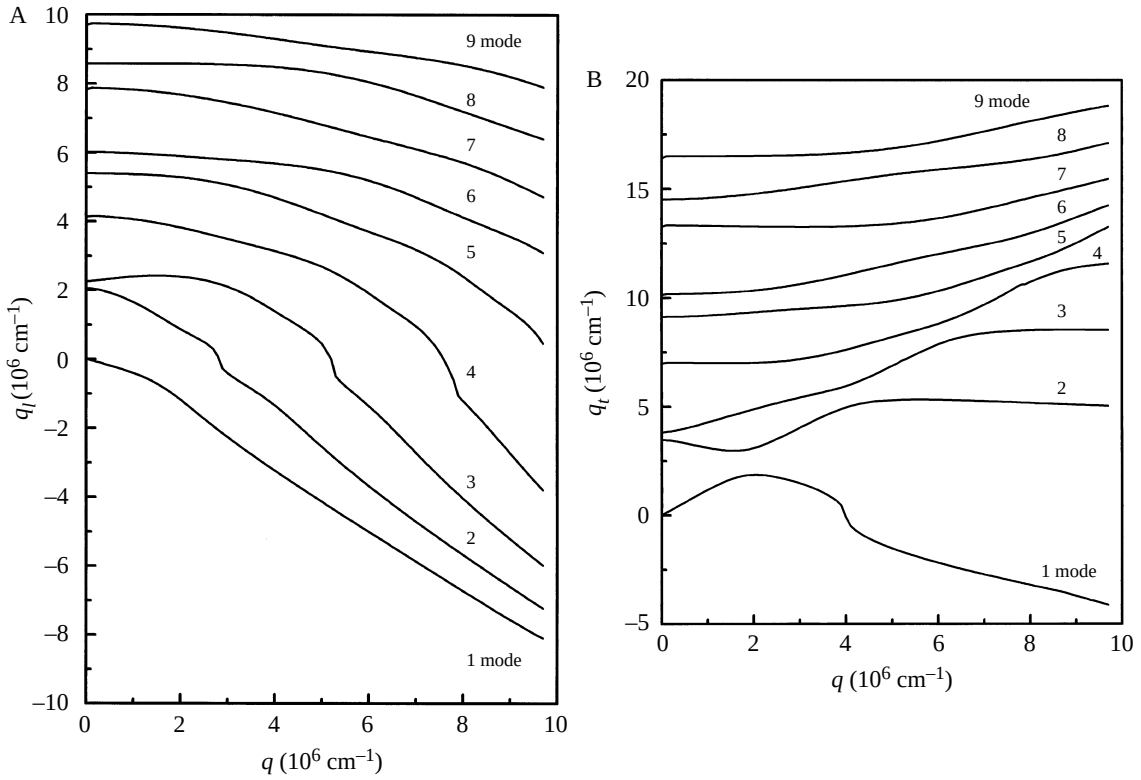

Fig. 2. Parameters A, q_l and B, q_t as functions of the in-plane vector q for the longitudinal modes in Si free-standing wire with diameter 200 Å. Several of the lowest order branches are depicted.

Substituting (8) into (11) and (12) we obtain relations between q, q_l and q_t for longitudinal wave in the case of free- and clamped-surface boundaries as outlined in Ref. [19]. Resulting equations have many solutions for q_l and q_t (at each particular q), which are continuous single-connected curves 'branches'. We label them with an additional index n : $q_{l,n}$ and $q_{t,n}$. These solutions will be either real or pure imaginary depending on q and n. In our case, we are interested in the real part of solutions corresponding to the propagating phonon modes which carry the heat.

4. Results of computations

Numerically solving transcendental equations [19], we find confined phonon modes for particular wire material parameters and dimensions. In Fig. 2A and B, we present an example of the $q_l \equiv q_l(q)$ and $q_t \equiv q_t(q)$ dependencies for longitudinal waves in the free-surface wire. The values of q_l and q_t above the abscissa are real; the values of q_l and q_t below the abscissa are imaginary. Using eqn (9), we plot the dispersion relations (see Fig. 3) for the longitudinal modes for the free-surface (solid lines) and clamped-surface (dashed lines) boundaries. The diameter of the silicon quantum wire is again $D = 200$ Å. The plot shows several branches of the lowest order. As the next step, the group velocity is then obtained by numerical differentiation. The phonon group velocity in the nth branch is defined as $v_g = /\partial\omega/\partial q/_n$.

In order to determine the lattice thermal conductivity we have to find phonon group velocity as a function of phonon frequency. The functional dependence of the phonon energy and group velocity on the

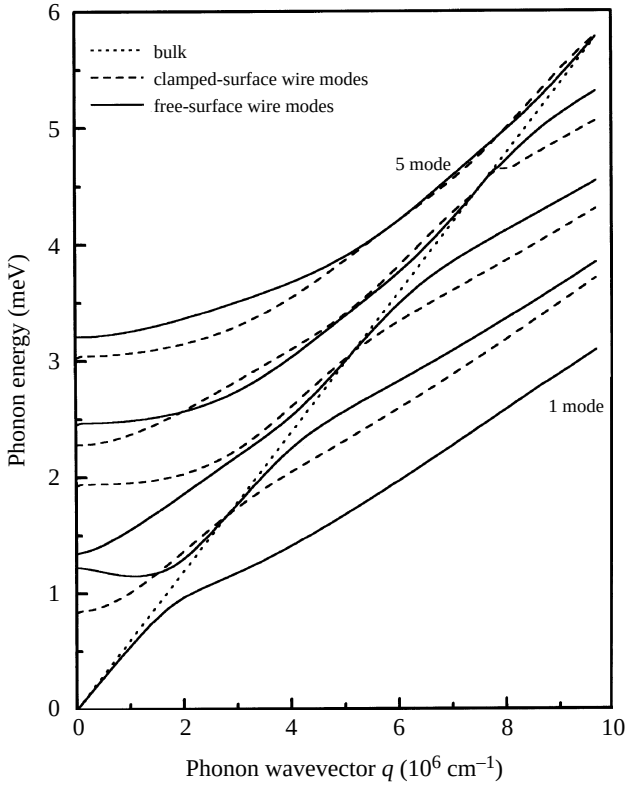

Fig. 3. The dispersion relation for longitudinal modes in Si wire of diameter 200 Å. Several branches of the lowest order are depicted. The free-standing surface corresponds to solid lines, the clamped-surface corresponds to dashed lines and the bulk corresponds to a dotted line.

phonon wavevector is important for calculation of the Umklapp scattering rates [17]. For evaluating the mass-difference scattering rates and boundary scattering rates in eqns (3) and (4), one needs to know the average phonon group velocity in the quantum wire. This velocity is expected to be different from that of the bulk. Figure 4 depicts the phonon group velocity in a quantum wire as a function of the phonon energy for several lowest modes. Different modes have different group velocities and the group velocity reaches the bulk sound velocity only in some specific very short energy intervals. In order to obtain the resulting group velocity we take the average group velocity as a function of phonon energy as follows,

$$\overline{v}_g(\hbar\omega) = \frac{\sum_n v_{g,n}(\hbar\omega) N_n(\omega)}{\sum_n N_n(\omega)}, \tag{13}$$

where $v_{g,n}$ is the group velocity of the nth mode, $N_n(\omega)$ is the number of oscillators with frequency ω on the nth mode. The Boltzmann equation was used to find the relation between the density of oscillators on nth and $(n+1)$th modes.

$$\frac{N_{n+1}}{N_n} \approx e^{-(\hbar\omega)/k_B T}. \tag{14}$$

Equation (14) is an approximation since we have a nonequidistant energy spacing for different phonon modes. The average group velocity obtained from (13) is depicted in Fig. 4 by a solid line. One can see that beginning with some phonon energy values, the average group velocity coincides with the first mode group velocity.

Table 1:

ρ	2.42×10^3 kg m^{-3}
$\Gamma \times 10^4$	2.64
M	46.6×10^{-27} kg
θ	625 K
γ	0.56
s_l	8.47×10^5 cm s^{-1}
s_t	5.34×10^5 cm s^{-1}
ω_0(Ge–Ge)	300 cm^{-1}

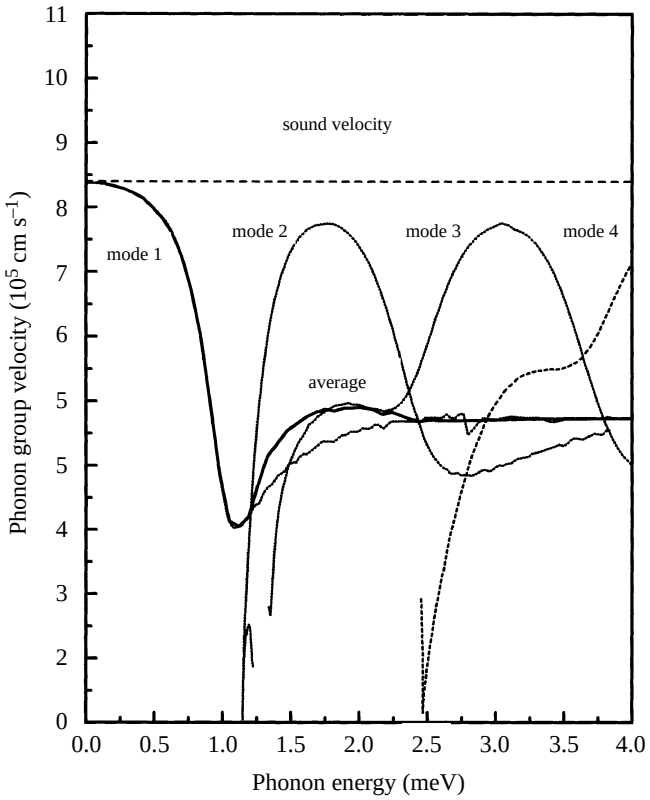

Fig. 4. Phonon group velocity as a function of phonon energy. A few first modes are depicted (dashed lines). The average group velocity is indicated as the solid line.

The overall value of the average phonon group velocity is only about half of the bulk phonon group velocity. In a bulk the phonon group velocity approximately coincides with the sound velocity for small values of the phonon wavevector. This is a significant drop.

Once we have found the average phonon group velocity over all contributing modes as a function of the phonon energy, we can obtain the lattice thermal conductivity using eqns (3)–(5). Material constants used for the simulation are summarized in Table 1. The relaxation rates due to the different scattering mechanism are shown in Fig. 5 as functions of phonon frequency. In Fig. 5 we separated the mass-different scattering to

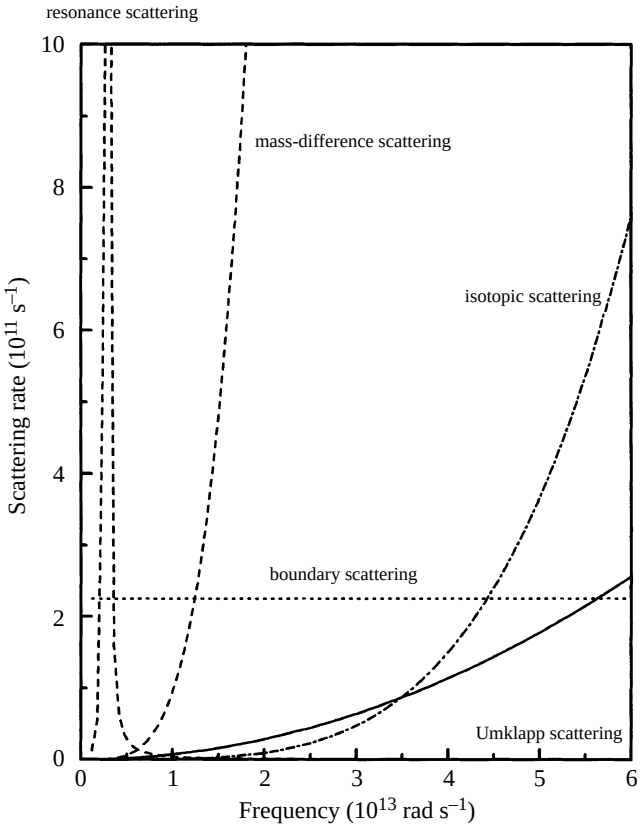

Fig. 5. Phonon relaxation rates due to different scattering mechanisms as functions of phonon frequency at $T = 300$ K.

the isotopic scattering, which is always present, and impurity (Ge) mass-different scattering. In the defect-free intrinsic bulk semiconductor the boundary, impurity (through mass difference) and resonant phonon scattering vanish. So that the thermal conductivity of the pure bulk silicon is determined only by the Umklapp and isotope scattering.

The scattering processes become more complicated in the presence of many impurity atoms. One can see the strong influence of mass-difference scattering on relaxation time in the presence of impurity with significantly different mass (as Ge with respect to Si). Beginning from early terahertz frequencies this different mass scattering became dominant. Resonance scattering mechanisms can also lead to a significant increase in relaxation time but its influence is localized in the vicinity of resonance frequency.

5. Discussion

In Fig. 6 we show the lattice thermal conductivity of a quantum wire as a function of temperature. The results are presented for the quantum wires with free- and clamped-surface boundaries as well as for the bulk material. The lattice thermal conductivity of the quantum wires is less than 10% of the bulk silicon value in the temperature range $T = 300$–700 K. This significant decrease in the thermal conductivity is the result of the increased isotope, Umklapp, and boundary–phonon scattering in a quantum wire. The latter comes from the modification of phonon dispersion due to spatial confinement. The change of the phonon modes

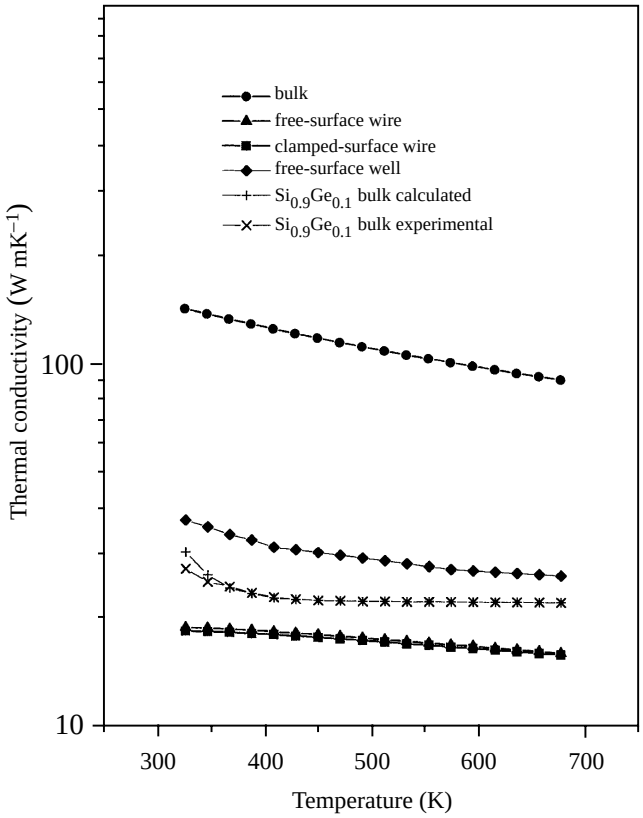

Fig. 6. Lattice thermal conductivity as a function of temperature for Si bulk material; Si free-surface well; $Si_{0.9}Ge_{0.1}$ bulk experimental obtained; $Si_{0.9}Ge_{0.1}$ bulk calculated, Si free-surface wire; Si clamped-surface wire.

leads to the reduction of the group velocity and, thus, increased phonon relaxation. Since the mass-difference scattering rate, which includes isotope scattering, is inversely proportional v_g^3, even small decreases of the phonon group velocity give rise to a strong increase in the phonon relaxation.

The important thing to notice here is that there is very little difference between the thermal conductivity of a free-standing quantum wire (free-surface boundaries) and a quantum wire embedded within rigid material (clamped-surface boundaries). This means that the effect is always pronounced provided that there is a well-defined distinct boundary between two materials of different elastic properties. The elastic properties can be characterized either by the characteristic phonon frequency ($\Omega(\mathrm{Si}) = 40.9\,\mathrm{meV}$) or acoustic impedence $K = \rho v$, where ρ is the density, and v is the bulk sound velocity. The small difference in thermal conductivity drop for free-surface and clamed-surface boundaries can be explained as follows. Although different boundary conditions lead to the different phonon dispersion modes and different energy spacing between them, the slop of each dispersion mode, which defines the group velocity, is very close in both cases and always smaller than that in the bulk.

We also calculated the lattice thermal conductivity of Ge-doped silicon quantum wires. As shown above, the lattice thermal conductivity is rather sensitive to the presence of the impurity atoms (via the mass-difference scattering mechanism). It was found that 10% mole fraction of Ge can decrease silicon bulk thermal conductivity by up to 10% of its initial bulk value. The experimental data point reported in Ref. [20] and our simulation data point are shown on Fig. 6. One should mention that the combination of two factors,

spatial confinement of phonons and presence of impurity atoms, can reduce the lattice thermal conductivity of a quantum wire by up to a few per cent of the bulk value of its constituent materials.

The decrease of the lattice thermal conductivity of an intrinsic quantum wire obtained in our case is much more severe than the one recently reported in Ref. [21]. The authors of Ref. [21] treated in detail the phonon–boundary scattering examining both diffusive and specular boundary scattering regimes. They found that the thermal conductivity drops five times (for a wire with 500 Å side) as compared with the bulk value. The decrease was attributed to the increased phonon–boundary scattering in the GaAs quantum wire. Although our results are qualitatively similar, we obtain a stronger decrease of the thermal conductivity due to the inclusion of phonon confinement effects. The discrepancy between these two-model descriptions is expected to be particularly big for narrow high-quality quantum wires embedded within material of different elastic properties. Under such conditions, the phonon modes are strongly confined and cannot be approximated with the regular bulk longitudinal and transverse modes.

Our data indicate that the decrease of the thermal conductivity in intrinsic free-standing quantum wires is larger than that which occurs in free-standing quantum wells of comparable size. Using the model for thermal conductivity of a free-standing quantum well developed by some of us earlier [17, 22], we found that at room temperature the following relation holds $k_{ph}(\text{wire})/k_{ph}(\text{well}) \sim 0.48$. This value was obtained for a cylindrical silicon quantum wire of diameter $D = 20$ nm and a rectangular silicon quantum well of thickness $W = 20$ nm. The ration of the wire to well thermal conductivity obtained on the basis of our model is close to the one obtained in Ref. [21] although the model approaches are significantly different.

The decrease of the thermal conductivity revealed in this work and its mechanism are in qualitative agreement with some recent experimental findings for thin silicon films and Si/Ge superlattices. Some of us have recently reported on the correlation between acoustic phonon folding in the small-period Si/Ge superlattices and the lattice thermal conductivity drop [23]. It was found that the thermal conductivity of the superlattice with the period 33 Å is 1.7 W mK^{-1} in the in-plane direction and 2.78 W mK^{-1} for the cross-plane direction, respectively. The obtained thermal conductivity was considerably lower than that determined using the bulk thermal conductivity values for Si, Ge, and $\text{Si}_x\text{Ge}_{1-x}$ alloys. This drop in thermal conductivity was attributed to the strong modification of the phonon modes (and corresponding phonon velocities) which lead to the phonon folding observed in the Raman spectra [23]. A giant drop in the lattice thermal conductivity (more than an order of magnitude) of the thin silicon film embedded within silicon nitride and silicon dioxide was reported by this group earlier [9].

Recent progress in fabrication of quantum wire arrays allows us to hope that such structures will soon be available for thermoelectric applications. One of the examples of such a structure is an array of Bi nanowires prepared using porous amorphous Al_2O_3 as a template [24]. The pores in amorphous Al_2O_3 are filled with Bi metal using a vacuum evaporation technique [24] or by the high-pressure liquid injection technique [25]. Another method of preparing quasi-periodic arrays of short nanowires of different materials using electrochemical deposition was reported in Ref. [26].

6. Conclusion

We have studied the effects of spatial confinement of the acoustic phonons on the lattice thermal conductivity in silicon quantum wires. Most of the heat in silicon structures is carried by acoustic phonons with the wavevectors close to the Brillouin zone center. In our analysis we rigorously took into account modification of the phonon modes and phonon group velocities in free- and clamped-surface wires due to spatial confinement. It has been shown that phonon confinement leads to a significant decrease (more than an order of magnitude) of the lattice thermal conductivity in cylindrical quantum wires with diameter $D = 200$ Å. The decrease is stronger in quantum wires than in quantum wells of corresponding dimensions and does not differ significantly for free- or clamped-surface boundaries. The predicted decrease of the lattice thermal conduc-

tivity is important for further development of Si/SiGe-based thermoelectric devices. The decrease may also complicate the heat management problem for future deep-submicron silicon-based devices and circuits.

Acknowledgements—The authors are indebted to Professor G. Chen (UCLA) and Professor M. S. Dresselhaus (MIT) for discussions on low-dimensional thermoelectrics. One of the authors (AB) thanks Professor P. G. Klemens (University of Connecticut) for discussions on thermal conductivity of semiconductors. This work was supported by the DoD MURI-ONR program on Thermoelectrics (Dr John Pazik) and DoD MURI-ARO program on Low Power Electronics (Dr James Harvey).

References

[1] T. Kojima, J. Xue-Ying, Y. Hayafune, and S. Tamura, Jpn. J. Appl. Phys. 1 **37**, 5961 (1998).
[2] V. S. Dneprovskii, E. A. Zhukov, E. A. Muljarov, and S. G. Tikhodeev, JETP **87**, 382 (1998).
[3] A. Forchel, P. Ils, K. H. Wang, and O. Schilling, Microelectron. Eng. **32**, 317 (1996).
[4] A. Svizhenko, A. Balandin, S. Bandyopadhyay, and M. A. Stroscio, Phys. Rev. **B57**, 4687 (1998).
[5] V. M. Fomin, V. N. Gladilin, J. T. Devreese, C. Van Haesendonck, and G. Neuttiens, Solid State Commun. **106**, 293 (1998).
[6] L. D. Hicks, T. C. Harman, and M. S. Dresselhaus, Appl. Phys. Lett. **63**, 3230 (1993).
[7] S. S. Kubakaddi and B. G. Mulimani, J. Appl. Phys. **58**, 3643 (1985).
[8] G. Chen and C. Tien, J. Thermophys. Heat Transfer **7**, 311 (1993).
[9] X. Y. Zheng, S. Z. Li, M. Chen, and K. L. Wang, *Micro-electro-mechanical Systems (MEMS)*, Proceedings of the ASME International Mechanical Engineering Congress and Exposition 1996 (ASME, New York, 1996) pp. 93–98.
[10] A. Balandin and K. L. Wang, J. Appl. Phys. **84**, 6149 (1998).
[11] A. Yamamoto, H. Kato, S. Kuwashiro, M. Takimoto, T. Ohta, K. Miki, K. Sakamoto, T. Matsui, and K. Kamisako, *Proceedings of the 16th International Conference on Thermoelectrics* (Dresden, Germany, 1997) (IEEE Cat. No. 97TH8291, ICT'97) p. 434.
[12] C. M. Bhandari, *CRC Handbook of Thermoelectrics*, edited by D. M. Rowe (Chemical Rubber Corporation, Boca Raton, FL, 1995) p. 55.
[13] P. G. Klemens, *Solid State Physics*, edited by F. Seitz and Turnbull (Academic, New York, 1958) Vol. 7, p. 1; Y.-J. Han and P. G. Klemens, Phys. Rev. **B48**, 6033 (1993).
[14] J. Callaway, Phys. Rev. **113**, 1046 (1959).
[15] G. P. Srivastava, *The Physics of Phonons* (Adam Hilger, New York, 1990) p. 175.
[16] M. Wagner, Phys. Rev. **131**, 1443 (1963).
[17] A. Balandin and K. L. Wang, Phys. Rev. **B58**, 1544 (1998).
[18] N. Bannov, V. Aristov, and V. Mitin, Phys. Rev. **B51**, 9930 (1995).
[19] SeGi Yu, K. W. Kim, M. A. Stroscio, and G. J. Iafrate, Phys. Rev. **B51**, 4695 (1995).
[20] J. P. Dismukes, L. Ekstrom, E. F. Steigmeier, I. Kudman, and D. S. Beers, J. Appl. Phys. **35**, 2899 (1964).
[21] S. G. Walkauskas, D. A. Broido, K. Kempa, and T. L. Reinecke, J. Appl. Phys. **85**, 2579 (1999).
[22] A. Balandin and K. L. Wang, *Nanostructures: Physics and Technology*, edited by Zh. Alferov *et al.* (Russian Academy of Sciences, St. Petersburg, Russia, 1998) pp. 24–27.
[23] J. Liu, A. Balandin, T. Borca-Tasciuc, Y. S. Tang, K. L. Wang, and G. Chen, *Proceedings of Materials Research Society, 1998, Boston, U.S.A.*, to appear.
[24] J. Heremans, C. M. Thrush, Z. Zhang, X. Sun, M. S. Dresselhaus, J. Y. Ying, and D. T. Morelli, Phys. Rev. **B58**, R10091 (1998).
[25] N. B. Brant *et al.*, Zh. Eksp. Teor. Fiz. **92**, 913 (1987) [Sov. Phys. JETP **65**, 515 (1987)].

[26] A. Balandin, S. Bandyopadhyay, P. G. Snyder, S. Stefanovich, G. Banerjee, and A. E. Miller, Phys. Low-Dim. Struct. **11/12**, 155 (1997).